





# Effective length of bamboo-like stiffened hollow cylindrical structures

Ryo Nishiyama <sup>1</sup> and Motohiro Sato <sup>2,\*</sup>

<sup>1</sup>Division of Mechanical and Space Engineering, Graduate School of Engineering, Hokkaido University, N-13, W-8, Kita-ku, Sapporo, Japan

<sup>2</sup>Division of Mechanical and Space Engineering, Faculty of Engineering, Hokkaido University, N-13, W-8, Kita-ku, Sapporo, Japan

\*Corresponding author: [tayu@eng.hokudai.ac.jp](mailto:tayu@eng.hokudai.ac.jp)

## ABSTRACT

Hollow cylindrical structures are susceptible to local buckling because they flatten and significantly reduce their stiffness when they bend. Therefore, many previous studies aimed to improve the strength of pipelines and building structures were conducted. Our research group has focused on bamboo and has theoretically proven that stiffness anisotropy caused by bamboo's unique nodes and vascular bundles enhances the stiffness of cylindrical structures. In this study, to investigate this analytically, we carried out a finite-element analysis and succeeded in deriving a new dimensionless parameter that the stiffening effect of an anisotropic consideration. This result is applicable to a wide range of cylindrical structures, from thin-walled to thick-walled, and it is expected that bamboo-inspired bionic designs will be proposed in the future.

**KEYWORDS:** hollow cylindrical structure, buckling, finite-element analysis, anisotropy

## 1. INTRODUCTION

Hollow cylindrical structures (e.g. pipes and tubes) are susceptible to bending, which causes local buckling. The latter arises because of a nonlinear geometric phenomenon in which the cross section flattens as a result of bending, and this significantly reduces the stiffness (i.e. the Brazier effect) [1]. To prevent such structural weaknesses in hollow cylinders and improve buckling resistance, Sato *et al.* proposed reinforcing the cross section with a double-tube structure and placing discrete ring stiffeners in the axial direction of the cylinder [2–4].

In addition to man-made structures, hollow cylindrical structures are found in nature. One example is bamboo [5–14], which is a plant with a unique node structure inside a cylinder (Fig. 1a). The nodes prevent the cross-sectional flattening caused by bending, and by varying the node spacing along its height, bamboo is able to achieve the strength necessary to maximize its height while minimizing its weight. This is one of the survival strategies that bamboo has acquired over a long period of time. The mechanical rationale for this nonuniform arrangement of nodes in the height direction was demonstrated theoretically by Shima *et al.* [15] using the dimensionless parameter,  $\Omega$ , which represents the cross-sectional stiffening effect demonstrated by Calladine [16]. Furthermore, by deriving  $\Omega$  in a way that accounts for anisotropy, it was shown that the anisotropic nature of the stiffness enhances the stiffening effect. The anisotropy is caused by the vascular bundle sheath (Fig. 1b), whose Young's modulus is in the order of several gigapascals, comparable to that of steel [17–19].

This cross-sectional stiffening effect at the edges propagates in the axial direction from the edges to the middle of the

cylinder; therefore, suppression of ovalization strongly depends on the cylinder length. Based on a buckling analysis, Rotter *et al.* [20–22] used an additional dimensionless parameter,  $\omega$ , to study the geometric nonlinearity of a perfectly elastic cylindrical shell subjected to uniform bending. According to the results, the buckling resistance due to terminal stiffening can be described by four behavioural regions (i.e. the relative lengths of the cylinders), in which  $\omega$  defines the properties of relatively short cylinders (“short” and “medium”) and  $\Omega$  defines the properties of relatively long cylinders (“transitional” and “long”).

In this study, it is shown that the  $\omega$  used by Rotter to classify the relative length of hollow cylinders can be derived from the effective length of the cross-sectional stiffening effect from the terminal, which is obtained from a finite-element analysis of the pure bending of hollow cylinders. In addition, we propose a new expression for  $\omega$  that is extended to consider anisotropy. This enables the length of a hollow cylinder with short anisotropy and that of an isotropic cylinder to be specified, which provides useful insights for structural design.

## 2. EFFECT OF CYLINDRICAL LENGTH ON NONLINEAR BUCKLING BEHAVIOUR

The buckling resistance of a cylinder is highly dependent on its geometric nonlinearity and its defects [21–23]. However, because this study considers a perfect cylinder with no initial irregularities, the elastic defect reduction factor  $\alpha_G$  can be expressed as the ratio of the nonlinear buckling moment  $M_k$  to the linear

Received: 5 March 2022; Accepted: 14 May 2022

© The Author(s) 2022. Published by Oxford University Press on behalf of Society of Theoretical and Applied Mechanics of the Republic of China, Taiwan. This is an Open Access article distributed under the terms of the Creative Commons Attribution License (<https://creativecommons.org/licenses/by/4.0/>), which permits unrestricted reuse, distribution, and reproduction in any medium, provided the original work is properly cited.

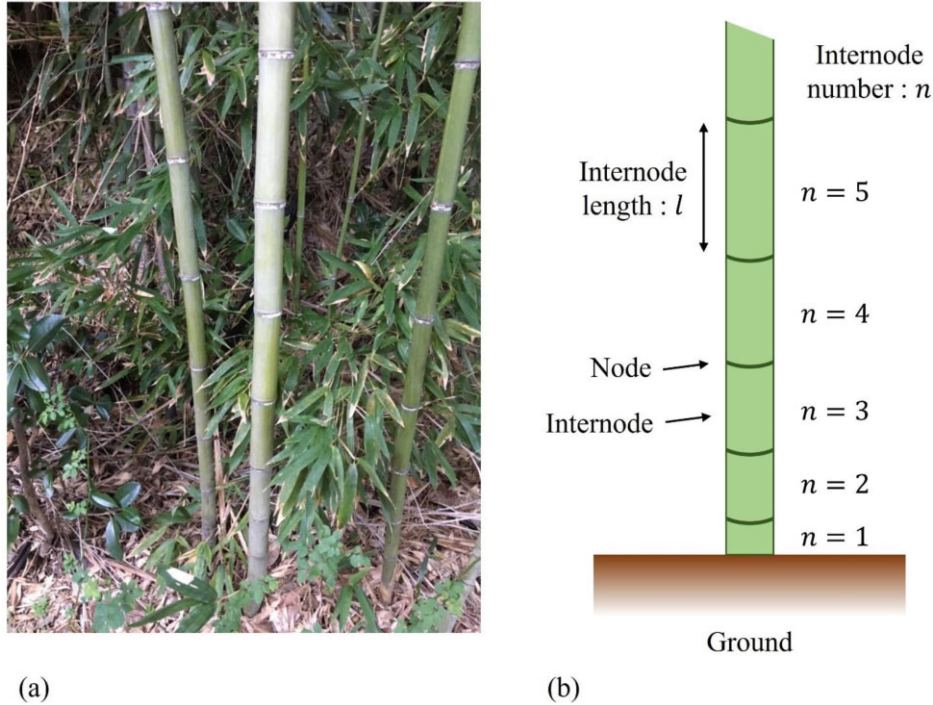


**Figure 1** (a) Wild bamboo grove. (b) Diagram of bamboo, showing its unique structure with multiple unevenly arranged nodes inside a cylinder.

**Table 1** Classification of the effect of cylinder length on nonlinear buckling behaviour [21–22].

Classification	Range	Limit point buckling/Features
Short	$\omega \leq 4.8$	$\alpha_G \gg 1$ $\alpha_G(\omega) = 1.93 - 0.5(\omega - 3.8)^2 - 0.44(\omega - 3.8)^3$ /Local buckling and ovalization are fully restrained by the boundary condition
Medium	$4.8 \leq \omega \leq 0.5 r/t$ $\Omega \leq 0.5$	$\alpha_G \approx 0.9$ /The $\sim 10\%$ reduction from $M_{cr}$ is caused by pre-buckling amplification of the edge boundary condition, as is also seen under axial compression. The resistance in this domain may be characterized as being relatively independent of $r/t$
Transitional	$\omega \geq 0.5 r/t$ $0.5 \leq \Omega \leq 7$	$0.5 \leq \alpha_G \leq 0.9$ $\alpha_G(\Omega) = 1.07 \left( \frac{1 - 0.22 \Omega + 0.061 \Omega^{2.94}}{1 + 0.12 \Omega^{2.94}} \right)$ /Increasing length permits progressively more ovalization and causes an increasingly nonlinear pre-buckling equilibrium path, leading to premature local buckling
Long	$\Omega \geq 7$	$\alpha_G \approx 0.5$ /Ovalization has developed fully

buckling moment  $M_{cr}$  as

$$\alpha_G = \frac{M_k}{M_{cr}}. \quad (1)$$

The effect of the cylindrical length on the nonlinear buckling behaviour can be classified into four regions based on  $\Omega$  and  $\omega$ , which are defined as [16, 20]

$$\Omega = \sqrt{\frac{tl^2}{r^3}}, \quad (2)$$

$$\omega = \frac{l}{\sqrt{tr}}, \quad (3)$$

respectively, where  $t$  is the cylinder wall thickness,  $r$  is the cylinder radius and  $l$  is the cylinder length. The detailed boundaries and characteristics of each region are listed in

Table 1. In the table, the boundary lengths of “medium” and “transitional” become shorter as the cylinder becomes thicker and is more strongly affected by geometric nonlinearities. According to Rotter *et al.* [21], the nonlinear elastic buckling moment  $M_k$  in each region is defined as

$$M_k = \alpha_G(\Omega, \omega) \left( 1 + \frac{4}{\omega^2} \right) 1.902Ert^2. \quad (4)$$

### 3. ANALYSIS

#### 3.1 Analysis model

To verify the mechanism by which a cylindrical bulkhead can reasonably resist a bending moment when subjected to pure bending, a model of a bamboo internode was constructed

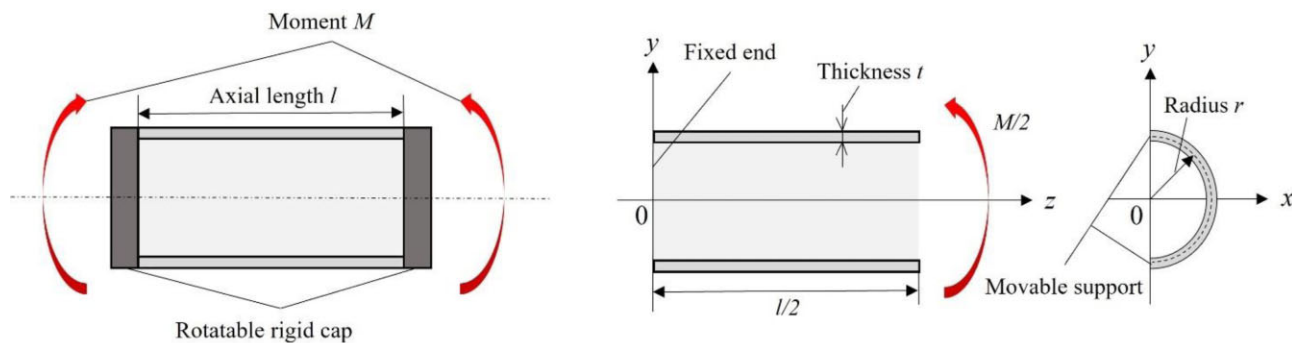


**Figure 2** (a) Specifications of the analysis model: uniform bending moments  $M$  were applied to both ends of a cylindrical shell defined by wall thickness  $t$ , radius  $r$  and length  $l$ . (b) The  $y$ - $z$  cross section of the analytical model (the moving support was placed in the  $y$ - $z$  plane to ensure symmetry); the fixed end acts as a rigid cap to prevent the cross section from bending. (c) The  $x$ - $y$  cross section of the analytical model; the radius  $r$  is defined by the neutral plane.

using ANSYS Workbench, a general-purpose finite-element analysis software. Figure 2a shows a single bamboo internode surrounded by knots. A rigid cap, which was free to rotate, was placed at both ends of the cylinder to serve as a bulkhead in the bamboo. To save elements, symmetry was utilized in the analytical model, as shown in Fig. 2b and c. The fixed end acts as a rigid cap to prevent the flat cross section from bending. Hexahedral quadratic elements were used to form the mesh, and the mesh size was adjusted according to the specifications of the analysis target to ensure accuracy.

### 3.2 Analysis conditions

In this analysis, the cylinder length  $l$  was set to 150 mm and the uniform bending  $M$  acting on the end of the cylinder was set to 1000 N mm.

#### 3.2.1 Material properties (isotropy)

A modulus of longitudinal elasticity of  $E = 200$  GPa and Poisson's ratio of  $\nu = 0.3$  were used. The analysis was performed by varying the thickness  $t$  and radius  $r$  to determine their respective contributions to the stiffening.

#### 3.2.2 Material properties (orthogonal anisotropy)

Bamboo can be regarded as a unidirectional fibre-reinforced composite material with a fibre structure known as a vascular bundle sheath (Fig. 3). Therefore, in this study, we assumed an orthotropic elastic material with a uniform cylindrical fibre distribution in the axial direction. In this case, the stress-strain relationship can be expressed by

$$\begin{bmatrix} \varepsilon_x \\ \varepsilon_y \\ \varepsilon_z \\ \gamma_{xy} \\ \gamma_{yz} \\ \gamma_{zx} \end{bmatrix} = \begin{bmatrix} 1/E_T & -\nu_{TT}/E_T & -\nu_{TL}/E_T & 0 & 0 & 0 \\ -\nu_{TT}/E_T & 1/E_T & -\nu_{TL}/E_T & 0 & 0 & 0 \\ -\nu_{LT}/E_T & -\nu_{LT}/E_L & 1/E_L & 0 & 0 & 0 \\ 0 & 0 & 0 & 1/G_{TT} & 0 & 0 \\ 0 & 0 & 0 & 0 & 1/G_{LT} & 0 \\ 0 & 0 & 0 & 0 & 0 & 1/G_{LT} \end{bmatrix} \begin{bmatrix} \sigma_x \\ \sigma_y \\ \sigma_z \\ \tau_{xy} \\ \tau_{yz} \\ \tau_{zx} \end{bmatrix} \quad (5)$$

where  $E_L$  and  $E_T$  are the longitudinal and transverse moduli, respectively;  $\nu_{LT}$ ,  $\nu_{TL}$  and  $\nu_{TT}$  are Poisson's ratios; and  $G_{LT}$  and  $G_{TT}$  are shear moduli.

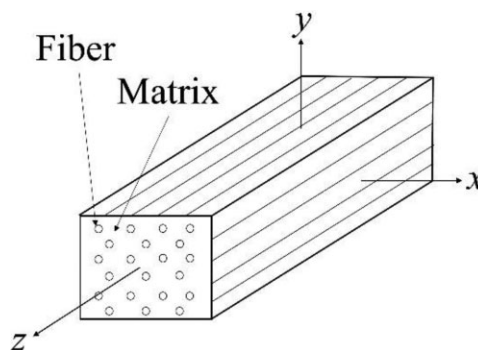


**Figure 3** Unidirectional fibre composite projected onto the  $(x, y, z)$  coordinate system; the  $z$ -direction is the fibre direction.

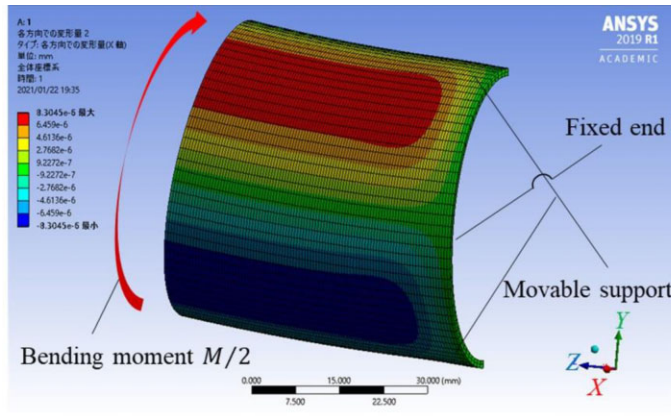
There were seven modulus components. Considering the symmetry of the matrix, as illustrated by auto

$$\frac{\nu_{LT}}{E_L} = \frac{\nu_{TL}}{E_T} \quad (6)$$

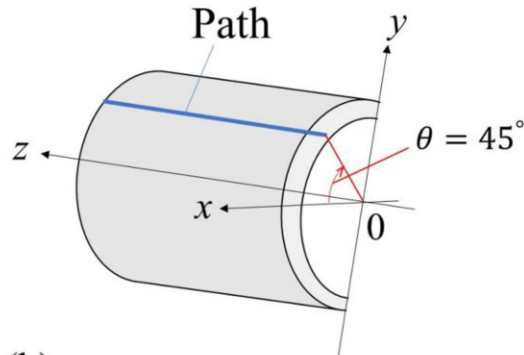
and

$$G_{TT} = \frac{E_T}{2(1 + \nu_{TT})}, \quad (7)$$

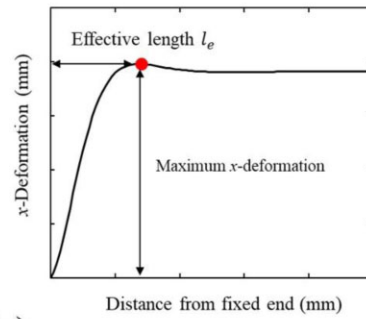
there were five independent components. In this analysis,  $E_T = 200$  GPa,  $\nu_{LT} = \nu_{TT} = 0.3$ ,  $G_{LT} = 76.9$  GPa, and only the longitudinal modulus  $E_L$  was used as a design variable for the material properties. The analysis was performed by varying the values of the wall thickness  $t$ , radius  $r$  and the longitudinal modulus to ascertain their contributions to the stiffening.



(a)

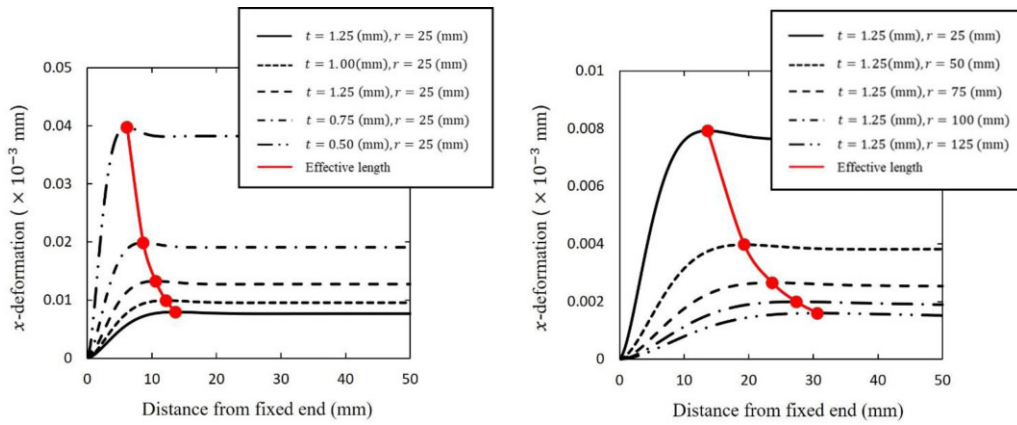


(b)



(c)

**Figure 4** (a) Analysis results produced by ANSYS Workbench for the  $x$ -deformation (in mm). (b) The flatness of the cross section was evaluated by the lateral protrusion of the cross section; the “path” was along the direction of the cylindrical axis on the  $x$ - $y$  plane at  $\theta = 45^\circ$ . (c) The  $x$ -deformation of the nodes along the “path” is plotted in panel (b).



(a) Effect of thickness  $t$

(b) Effect of radius  $r$

**Figure 5** Relationship between  $x$ -deformation and the distance from the fixed end: effect of (a) varying the thickness  $t$  while fixing the radius  $r$  at 25 mm and (b) varying  $r$  while fixing  $t$  at 1.25 mm.

### 3.3 Evaluation

Figure 4a shows an example of the analysis results, showing the  $x$ -deformation due to bending. The contour plot indicates that the deformation was large at  $\theta = 45^\circ$ . Therefore, a “path” was created in the direction of the cylinder length at  $\theta = 45^\circ$  (see

Fig. 4b), and the magnitude of the  $x$ -deformation at the nodes on this “path” is plotted in Fig. 4c. Additionally, the length from the fixed end to where the deformation was at its maximum is defined as the effective length  $l_e$ , and this parameter was used to evaluate the stiffening.

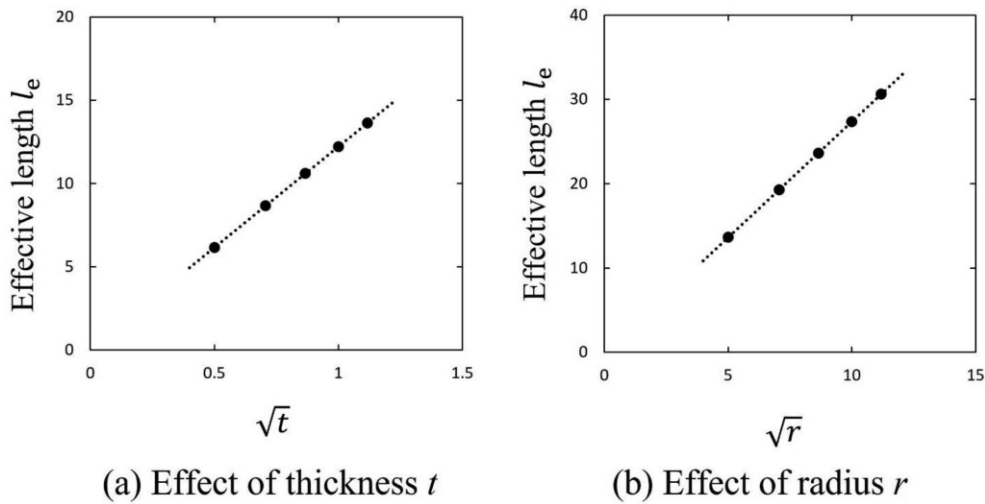


Figure 6 Change in the effective length of the cross-sectional stiffening effect from the terminal as a function of (a) thickness  $t$  and (b) radius  $r$ .

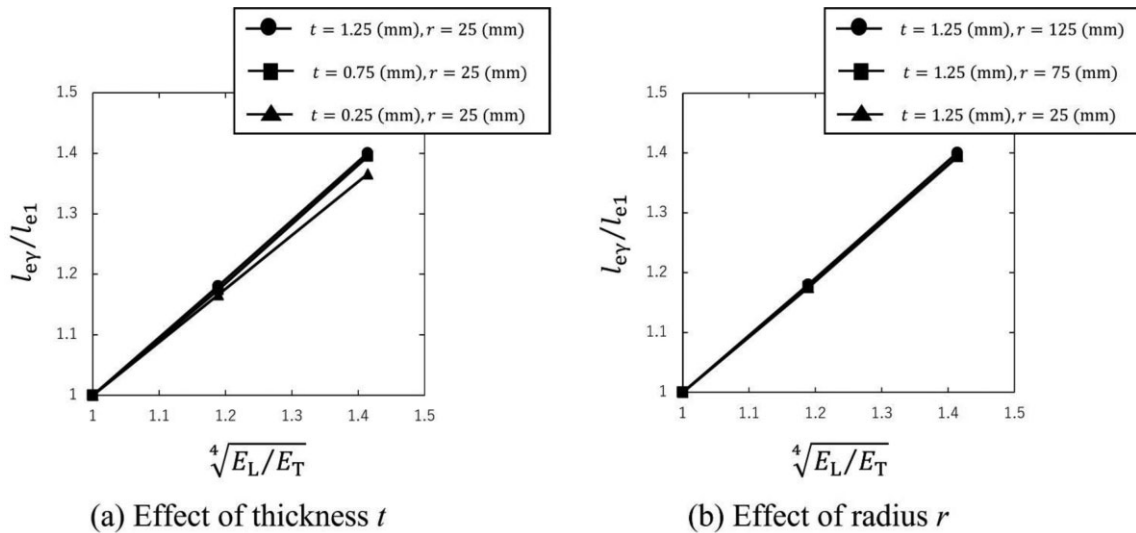


Figure 7 Elongation of the effective length of the cross-sectional stiffening effect from the terminal caused by the anisotropy of the material: (a) effect of thickness  $t$  and (b) effect of radius  $r$ .

## 4. RESULTS

### 4.1 Isotropic elasticity

To investigate the effective length of the stiffening (see Fig. 5a), the changes in the  $x$ -deformation were investigated by fixing the radius  $r$  at 25 mm and varying the wall thickness  $t$  to the values of 0.25, 0.50, 0.75, 1.00 and 1.25 mm. In addition, the wall thickness  $t$  was fixed at 1.25 mm, and the radius  $r$  was set to the values of 25, 50, 75, 100 and 125 mm (see Fig. 5b). Because the effective length  $l_e$  is proportional to  $\sqrt{t}$  and  $\sqrt{r}$  (see Fig. 6), the effective length  $l_e$  of the complementary effect of the terminal constraint can be expressed by

$$\frac{l_e}{\sqrt{tr}} \approx 2.45. \tag{8}$$

If  $l = 2l_e$ , the right-hand side of Eq. (8) corresponds to  $\omega$ . In this case, the stiffening effect extended to the entire cylinder, and the constant in Eq. (8) corresponded to the “short” region.

Rotter defined this boundary length as “the region where local buckling and ellipticity are completely suppressed by the boundary condition,” and our analysis successfully confirmed this from a cross-sectional deformation perspective.

### 4.2 Orthogonal anisotropy

The ratio of the longitudinal modulus to the transverse modulus is called the modulus ratio:  $\gamma = E_L/E_T$ . In this case, the effective length is denoted by  $l_{e\gamma}$ . For example, if we assume that the material is isotropic elasticity ( $E_L = E_T$ ), then  $\gamma = 1$  and  $l_{e\gamma} = l_{e1}$ . To verify the effect of the anisotropy of the material on the stiffening, the thickness  $t$  and radius  $r$  of the cylinder were varied accordingly.

As shown in Fig. 7,  $l_{e\gamma}/l_{e1}$  is proportional to  $\sqrt[4]{E_L/E_T}$ . Using the linear approximation with the least-squares method,  $l_{e\gamma}/l_{e1} = \sqrt[4]{E_L/E_T}$  is derived. This does not depend on the combination of  $t$  and  $r$ . In addition to the above results, based on

Eq. (8) and the second paragraph of Section 4.1, the anisotropic consideration  $\omega'$  can be derived as

$$\omega' = \sqrt[4]{\frac{E_T}{E_L}} \frac{l}{\sqrt{tr}}. \quad (9)$$

As the cylinders became thicker, they became more susceptible to geometric nonlinearities and relatively less resistant to buckling. Therefore, the anisotropy of the cylindrical material enhanced the effect of terminal stiffening of the cylinder and strengthened its resistance to buckling. The fact that the stiffening effect increased in proportion to the one-fourth power of the modulus ratio was also observed for the anisotropic  $\Omega$  [15]. It is expected that both findings will be combined to derive nonlinear elastic buckling moments by accounting for anisotropy.

## 5. CONCLUSIONS

In this study, it was shown that the  $\omega$  used by Rotter to classify the relative length of hollow cylinders can be derived from the effective length of the cross-sectional stiffening effect from the terminal, which was obtained from a finite-element analysis of the pure bending of a hollow cylinder. Furthermore, by focusing on the unique knot and vascular bundle structure of bamboo, we derived  $\omega$  by considering the anisotropy and clarified that the anisotropy of the stiffness enhanced the complementary effect of the cylindrical terminal. This enabled the length of a short hollow cylinder with anisotropy and that of an isotropic cylinder to be specified. In the future, we will address the detailed buckling analysis of hollow cylinders with anisotropic materials, and an expression for the nonlinear bifurcation moment that considers anisotropy will be derived based on the knowledge obtained from this study. And it will provide useful information for the design of hollow cylindrical structures such as electricity poles, horizontal tanks, pipelines, tubular piles and wind turbine support towers.

## ACKNOWLEDGMENTS

We acknowledge Profs. A. Inoue and H. Shima for helpful discussions. This work was supported by JSPS KAKENHI, Japan Grant Number 18H03818.

## AUTHOR CONTRIBUTIONS

R.N. and M.S. conceived and designed the study, contributed to the development of the methods and conducted the analysis and interpretation. R.N. contributed to the literature collection, formulation, numerical calculations and manuscript preparation. M.S. supervised the postgraduate research thesis of R.N.

## CONFLICT OF INTEREST

The authors declare no competing interests.

## REFERENCES

1. Brazier LG. On the flexure of thin cylindrical shells and other thin sections. *Proceedings of the Royal Society of London* 1927;**A116**: 104–114.
2. Sato M, Ishiwata Y. Brazier effect of single- and double-walled elastic tubes under pure bending. *Structural Engineering and Mechanics* 2015;**53**(1);17–26.
3. Sato M, Patel MH, Trarieux F. Static displacement and elastic buckling characteristics of structural pipe-in-pipe cross-sections. *Structural Engineering Mechanics* 2008;**30**(3): 263–278.
4. Sato M, Patel MH. Exact and simplified estimations for elastic buckling pressures of structural pipe-in-pipe cross sections under external hydrostatic pressure. *Journal of Marine Science and Technology* 2007;**12**(4):251–262.
5. Tan T, Rahbar N, Allameh SM, Kwofie S, Dissmore D, Ghavami K, Soboyejo WO. Mechanical properties of functionally graded hierarchical bamboo structures. *Acta Biomaterialia* 2011;**7**(10):3796–3803. <https://www.ncbi.nlm.nih.gov/pubmed/21704742>.
6. Clark LG, Londoño X, Ruiz-Sanchez E. Bamboo taxonomy and habitat. *Tropical Forestry* 2015;1–30. [10.1007/978-3-319-14133-6\\_1](https://doi.org/10.1007/978-3-319-14133-6_1).
7. Habibi MK, Samaei AT, Gheshlaghi B, Lu J, Lu Y. Asymmetric flexural behavior from bamboo's functionally graded hierarchical structure: underlying mechanisms. *Acta Biomaterialia* 2015;**16**:178–186. <https://www.ncbi.nlm.nih.gov/pubmed/25662164>.
8. Honfo H, Tovissodé FC, Gnanglè C, Mensah S, Salako VK, Assogbadjo AE, Agbangla C, Kakai RG. Traditional knowledge and use value of bamboo in Southern Benin: implications for sustainable management. *Ethnobotany Research Applications* 2015;**14**: 139–153.
9. Liu S, Tong Z, Tang Z, Liu Y, Zhang Z. Bionic design modification of non-convex multi-corner thin-walled columns for improving energy absorption through adding bulkheads. *Thin Walled Structures* 2015;**88**:70–81.
10. Sun Y, Sills RB, Hu X, Seh ZW, Xiao X, Xu H, Luo W, Jin H, Xin Y, Li T, Zhang Z, Zhou J, Cai W, Huang Y, Cui Y. A bamboo-inspired nanostructure design for flexible, foldable, and twistable energy storage devices. *Nano Letters* 2015;**15**(6):3899–3906. <https://www.ncbi.nlm.nih.gov/pubmed/26011653>.
11. Zou M, Xu S, Wei C, Wang H, Liu Z. A bionic method for the crashworthiness design of thin-walled structures inspired by bamboo. *Thin Walled Structures* 2016;**101**: 222–230.
12. Sato M, Inoue A, Shima H. Bamboo-inspired optimal design for functionally graded hollow cylinders. *PLoS One* 2017;**12**(5):e0175029. <https://www.ncbi.nlm.nih.gov/pubmed/28467441>
13. Palombini FL, de Araujo Mariath JE, Freitas de Oliveira B. Bionic design of thin-walled structure based on the geometry of the vascular bundles of bamboo. *Thin Walled Structures* 2020;**155**: 1–12.
14. Nishiyama R, Sato M. Structural rationalities of tapered hollow cylindrical beams and their use in Japanese traditional bamboo fishing rods. *Science Reports* 2022;**12**(1):2448.
15. Shima H, Sato M, Inoue A. Self-adaptive formation of uneven node spacings in wild bamboo. *Physical Review E* **93**(2):022406. [Doi:10.1103/PhysRevE.93.022406](https://doi.org/10.1103/PhysRevE.93.022406).
16. Calladine C. *Theory of Shell Structures*. Cambridge: Cambridge Univ. Press, 1983.
17. Shao Z-P, Fang C-H, Huang S-X, Tian G, Tian G-L. Tensile properties of Moso bamboo (*Phyllostachys pubescens*) and its components with respect to its fiber-reinforced composite structure. *Wood Science and Technology* 2010;**44**(4): 655–666.
18. Youssefian S, Rahbar N. Molecular origin of strength and stiffness in bamboo fibrils. *Science Reports* 2015;**5**(1):11116.
19. Shang L, Sun Z, Liu X, Jiang Z. A novel method for measuring mechanical properties of vascular bundles in moso bamboo. *Journal of Wood Science* 2015;**61**(6):562–568.
20. Rotter JM. Cylindrical shells under axial compression. In Teng JG, Rotter JM (ed). *Buckling of Thin Metal Shells*. Spon Press, London, pp. 42–87, 2004.

21. Rotter JM, Sadowski AJ, Chen L. Nonlinear stability of thin elastic cylinders of different length under global bending. *International Journal of Solids and Structures* 2014;**51**(15–16): 2826–2839.
22. Wang J, Kunle Fajuyitan O, Orabi MA, Rotter JM, Sadowski AJ. Cylindrical shells under uniform bending in the framework of Reference Resistance Design. *Constr Steel Res* 2020;**166**: 105920.
23. Fajuyitan OK, Sadowski AJ, Rotter JM. A study of imperfect cylindrical steel tubes under global bending and varying support conditions, *Proc 8th Int Conf on Advances in Steel Structures*. Lisbon, Portugal, 2015.